Buckling of elliptical cylindrical shell with variable circumferential thickness under fluid lateral pressure

Davood Poorveis [*,1], Amin Khajehdezfuly [1],Masoud Oulapour [1], Hakim Tamimi [1]

1. Department of Civil Engineering, Faculty of Civil Engineering and Architecture, Shahid Chamran University of Ahvaz, Ahvaz, Iran.

***Corresponding Author:**
Davood Poorveis,

Email: dpoorveis@scu.ac.ir
Received: 2025.08.10
Accepted: 2025.09.21
J. Hydraul. Struct., 2025; 12(3):1-18
DOI: 10.22055/jhs.2025.50371.1361

ABSTRACT

A review of the literature indicates that, due to the uniform curvature of circular cross-sections, the buckling load of elliptical cylindrical shells subjected to fluid lateral pressure is significantly lower than that of their circular counterparts. In many cases, fluid pressure is treated as follower pressure, meaning that the direction of the pressure exerted on an object changes in accordance with its deformation. In this study, to enhance the buckling capacity of elliptical shells, the shell thickness is varied along the circumferential direction, with greater thickness assigned to regions of lower curvature. Three thickness variation patterns (including power-law, exponential, and logarithmic) were considered in this study. A finite strip model of the shell was developed, and the buckling load was determined using the eigenvalue method. The accuracy of the developed model was validated by comparison with results obtained from finite element analysis. A comprehensive parametric study was conducted to assess the effect of geometric parameters and thickness variation patterns on the buckling of elliptical shells with circumferentially variable thickness. The results demonstrated that employing exponential, power-law, and logarithmic thickness variation can increase the buckling load by approximately 70, 60, and 20 percent, respectively. Furthermore, it was shown that for shells with a length-to-radius ratio greater than 16, the difference in buckling load under follower versus non-follower lateral pressure exceeds 30% in the most cases.

KEYWORDS

Elliptical cylindrical shell, Variable circumferential thickness, fluid pressure, follower lateral pressure, buckling.

1. Introduction

Cylindrical shells have been widely used in marine structures, the aerospace and missile industries, and pressure vessels [1]. A review of the literature indicates that assessing the buckling and stability of shells under lateral pressures and axial compressive loads is one of the most critical design criteria for these structures [2-3]. Accordingly, the buckling and stability of the shell structures have been assessed in numerous numerical and experimental previous works. Prior research has proposed various methods to enhance the buckling load of shells, including the replacement of isotropic materials with anisotropic ones (such as composite materials and Functionally Graded Materials (FGMs)) and the use of longitudinal and circumferential stiffeners [4-6].

However, these approaches often lead to a significant increase in construction costs due to the use of larger volumes of material (stiffeners) or higher-quality materials (composites and FGMs).
Alternatively, varying the shell thickness along the longitudinal or circumferential direction is another effective method for improving stability and increasing the buckling load. Although this method requires specific manufacturing technologies, it does not involve the use of special materials (such as composites or FGMs) or additional materials (like stiffeners) to enhance the shell's load-bearing capacity. A review of previous studies reveals that extensive research has focused on the effect of longitudinal thickness variations on the buckling and stability of cylindrical shells. For example, Aksogan and Sofiyev [7] employed Galerkin's method and a Ritz-type approach to investigate the dynamic buckling of elastic cylindrical shell with longitudinally varying thickness under uniform external pressure. In their study, the shell thickness was varied according to linear, parabolic, and exponential patterns. Jabbari et al., [8] applied higher-order shear deformation theory (HSDT) and a multilayer approach to develop a semi-analytical solution for the thermoelastic analysis of Functionally Graded (FG) cylindrical pressure vessels with variable longitudinal thickness subjected to non-uniform internal pressure. Three thickness profiles, linear, concave and convex, were considered in their analysis. Fan et al., [9] employed Sachenkov–Baktieva method and Fourier series expansion to study the dynamic buckling of cylindrical shells having arbitrary axisymmetric thickness variations in the longitudinal direction under time-dependent axial pressure. Ghareghani et al., [10] analyzed the bending and buckling behavior of clamped–clamped FGM cylindrical shells with longitudinally varying thickness using modified couple stress theory. Bacciocchi et al., [11] performed a free vibration analysis of plates and shells with longitudinal thickness variations using the generalized differential quadrature method.
Aghajari et al., [12] conducted experimental and numerical investigations on the buckling and post-buckling behavior of thin-walled cylindrical steel shells with variable longitudinal thickness under uniform external pressure. Chen et al., [13] examined the buckling of cylindrical shells under axial compression with small arbitrary thickness variations along the axial direction. Their study considered three types of thickness variation: stepwise, local and axisymmetric patterns. Selahi et al., [14] proposed a hybrid approach, comprising layer-wise theory, the Fourier series expansion and differential quadrature approach, for transient analysis of FG truncated conical longitudinally variable-thickness shells subjected to asymmetric dynamic pressure. Sofiyev [15] used Galerkin and Ritz methods to study the buckling of truncated conical composite thickness-variable shells under uniform pressure. Ghannad et al., [16] utilized a perturbation-based approach to investigate the buckling of a fixed-fixed thick FGM cylindrical shells with longitudinal thickness variation under internal pressure. Fazlalipour and Showkati [17] investigated the buckling behavior of variable-thickness steel cylindrical shells under combined loading. They employed a stepwise thickness variation along the longitudinal direction. Bakulin and Nedbai [18] applied the Bubnov–Galerkin method to assess the stability of a composite cylindrical variable-thickness shell subjected to axial and external pulsing pressures. Mahboubi Nasrekani and Eipakchi [19] examined the buckling of axisymmetric cylindrical shells with inhomogeneous longitudinal thickness under axial compression based on first-order shear deformation theory. Finally, Ghasemi and Hajmohammad [20] evaluated the buckling and post-buckling of variable-thickness cylindrical shells under external hydrostatic pressure.

On the other hand, comparatively few studies have explored the effect of

circumferential thickness variations on shell buckling and stability. Khalifa Ahmed [21] investigated the buckling of a variable-thickness cylindrical shell (varying thickness through circumferential direction) subjected to inhomogeneous circumferentially compressive pressures. Khalifa Ahmed [22] studied the vibration of an elastic oval cylindrical shell with varying circumferential thickness. In the study conducted by Khalifa Ahmed [22], the thickness change was such that the smaller the curvature, the greater the thickness. Gusic et al., [23] evaluated the buckling of harmonically-thickness-variable thin cylindrical shell subjected to external pressure via finite element analysis. Yang et al., [24] developed a theoretical approach for investigating the buckling of cylindrical shells having non-axisymmetric thickness variations along with longitudinal and circumferential directions under lateral pressure. Feng et al., [25] and Yang [26] investigated the buckling of cylindrical shells with arbitrary circumferential thickness variations (as an imperfection) under external pressure. Although these works provide useful insights, they remain largely descriptive and focused on specific loading or geometry cases. A clear synthesis indicates that circumferential thickness variation has not been systematically examined as a deliberate design strategy but rather as an imperfection or secondary parameter. More importantly, while some attention has been given to circular shells, the situation for elliptical shells remains understudied.

A review of the literature indicates that the buckling load of an elliptical shell is significantly lower than that of a circular shell [27]. In regions of the oval cross-section where the curvature is lower, the bending stiffness is reduced, making those areas more susceptible to local buckling under applied loads. Furthermore, no studies to date have investigated the use of circumferential thickness variation as a means of enhancing the buckling load of elliptical shells. This demonstrates a critical knowledge gap: although elliptical shells are more vulnerable to buckling, no studies to date have investigated whether circumferential thickness variation can be used to counteract this weakness and enhance their load-bearing capacity. In this study, while the total material volume of the shell structure is kept constant, the shell thickness at each point along the oval cross-section is defined as a function of the curvature. Specifically, points with greater curvature are assigned smaller thickness values. Accordingly, three Thickness Variation Patterns (TVPs) including power, logarithmic, and exponential, were considered in the circumferential direction. An elliptical cylindrical shell model with variable thickness was developed using the finite strip method. The model's results were validated by comparing them with data from the literature. A parametric study was then conducted to evaluate the effect of circumferential thickness variation on the buckling lateral pressure of the elliptical shell.

2. Development of model

Figure 1 shows the oval cross section with variable thickness in circumferential direction simulated in this study. The maximum and minimum diameters of the oval section are a and b, respectively. According to figure 1, as the curvature decreases, the thickness of the shell increases. So, the minimum thickness (hmin) is considered at the highest curvature of the oval section. Z-Y and n-θ stand for vertical-horizontal and normal-tangential coordinate systems, respectively. As shown in figure 1, the angle and radius of curvature of an arbitrary point located at the mid-plane of the ellipse are θ and $R(\theta)$, respectively. The thickness of the ellipse at this point is considered as $h(\theta)$. Equation 1 provides the relationship between the radius of curvature and other geometric variables of the elliptical cross-section (including a, b and θ) [28].

$$R(\theta) = \frac{a^2 b^2}{(a^2 \cos^2(\theta) + b^2 \sin^2(\theta))^{3/2}} \quad (1)$$

In equation 1, b and a stand for the minimum and maximum radii of the oval section (Figure 1). Moreover, θ and $R(\theta)$ were defined earlier. Figure 2 shows a 3D view of a variable-thickness elliptical cylindrical shell subjected to fluid lateral pressure. The shell's cross-section is depicted in Figure 1. In this study, the shell was discretized into several finite strip elements. To achieve this, a strip element with variable thickness in the transverse direction was developed, as illustrated in Figure 3. Additionally, Figure 4 shows the placement of the curved strip element on the positive quarter of the elliptical cross-section.

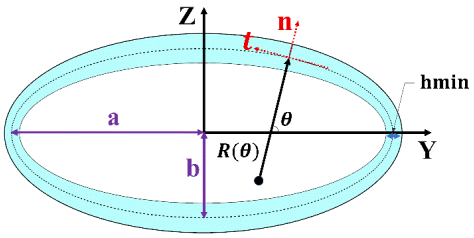


Figure 1. Oval cross section with variable thickness in circumferential direction

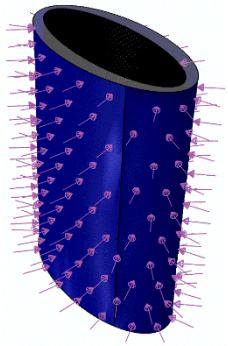


Figure 2. Variable-thickness elliptical cylindrical shell under fluid lateral pressure

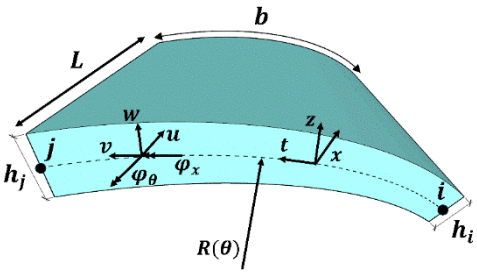


Figure 3. 3D view of finite strip element developed in this study

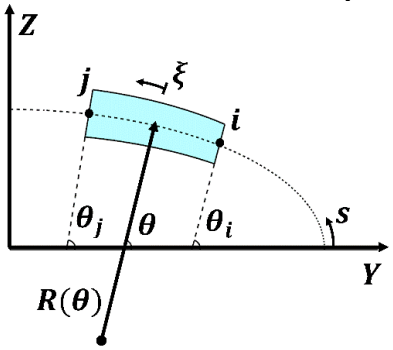


Figure 4. Curved strip element position on positive quarter of ellipse cross-section

Figure 3 shows 3D view of a strip element with length of L, width of b, variable thickness ($h(\theta)$) and variable radius of curvature ($R(\theta)$). As presented in figures 3, two nodes (i and j) were considered to develop Lagrangian shape functions in the transverse direction. The thickness of the element in nodes i and j is h_i and h_j , respectively. Figure 4 shows a two-noded strip element with variable thickness along with the global and local coordinates (s, ξ). As illustrated in figure 4, local coordinate of ξ is zero at the middle of the strip width and changes from -1 to +1. The radius of curvature at i and j nodes of the strip element were calculated based on θ_i and θ_i and via Equation 1. Also, the shape functions in elliptical cross-section are extracted using equation 2 [29].

$$\begin{aligned} \mathrm{N}_1(\xi) &= \frac{1-\xi}{2} \\ \mathrm{N}_2(\xi) &= \frac{1+\xi}{2} \end{aligned} \tag{2}$$

In equation 2, $\mathrm{N}_1(\xi)$ and $\mathrm{N}_2(\xi)$ are shape functions of nodes i and j, respectively, at ξ *coordinate*. Accordingly, the value of each variable at coordinate of ξ (f(ξ)) is calculated using equation 3 [29].

$$\mathrm{f}(\xi) = \mathrm{N}_1(\xi)\mathrm{f_i} + \mathrm{N}_2(\xi)\mathrm{f}_j \tag{3}$$

In equation 3, f_i and f_j are the value of the variable at nodes i and j, respectively. Accordingly, equation 4 was used to calculate the arc length of a point in ξ local coordinate ($s(\xi)$) based on arc lengths of points i and j (s_i and s_j) [29]. Following sub-sections present the details of the finite strip model developed in this study.

$$s(\xi) = s_i N_1(\xi) + s_j N_2(\xi) \quad (4)$$

2.1. Thickness variation in strip element

In this study, the change in shell thickness in the circumferential direction is considered in such a way that the volume of material used in the shell does not change compared to a shell with a constant thickness. This hypothesis has become the basis for considering logical patterns for thickness variation, such that in areas with lower curvature, the shell thickness is increased in order to reduce stress, and in contrast, in areas with higher curvature, the shell thickness is decreased to balance the bending stiffness across the entire cross section. In this study, three distinct patterns were considered for variation of the thickness along with the circumferential direction (including power, exponential and logarithmic). It is important to note that the power value of power TVP includes various thickness distributions, including linear and quadratic.

2.1.1. Power thickness variation

Equation 5 shows the power variation in thickness of strip element based on the change in the curvature.

$$\Delta h = \alpha \left(\frac{R(\theta)}{R_{min}}\right)^n + \beta \quad (5)$$

In Equation 5, Δh represents the difference between the thickness at a point with curvature radius $R(\theta)$ and the minimum thickness of the elliptical section (which is hmin as shown in Figure 1). Moreover, R_{min} denotes the curvature radius of the point with the minimum thickness (hmin) and n is the power value and can take positive real values. Accordingly, the coefficients α and β were determined such that Δh=0 when $R(\theta) = R_{min}$. The coefficient α was also calculated under the assumption that the volume of the cylinder material remains constant. In this study, the perimeter of the ellipse is considered constant. Due to the symmetry of the elliptical shell with respect to both the major and minor axes, calculations were performed for only one-fourth of the elliptical cross-section. Accordingly, the thickness at the point with curvature radius of $R(\theta)$ is expressed as follows:

$$h(\theta) = hmin + \alpha \left[\left(\frac{R(\theta)}{R_{min}}\right)^n - 1\right] \quad (6)$$

In equation 6, $h(\theta)$ is thickness at curvature angle of θ. By assuming an equivalent circular section with constant thickness h_0 and equivalent radius R_0, the following constraint is obtained:

$$\int_0^{\frac{\pi}{2}} h(\theta) R(\theta)\, d\theta = \frac{\pi R_0 h_0}{2} \quad (7)$$

In this research, the values of R_0 and h_0 are 100 and 1, respectively. Equation 7 is expanded as follows:

$$-\alpha \int_0^{\frac{\pi}{2}} R(\theta)\, d\theta + \alpha \left(\frac{1}{R_{min}}\right)^n \times \int_0^{\frac{\pi}{2}} R_{(\theta)}^{n+1}\, d\theta + \frac{\pi R_0 hmin}{2} = \frac{\pi R_0 h_0}{2} \quad (8)$$

Accordingly, α is obtained as A_1/A_2, where A_1 and A_2 are obtained using equation 9.

$$A_1 = \frac{\pi R_0}{2}(h_0 - hmin)$$
$$A_2 = \left(\frac{1}{R_{min}}\right)^n \times \int_0^{\frac{\pi}{2}} R(\theta)^{n+1}\, d\theta - \frac{\pi R_0}{2} \quad (9)$$

2.1.2. Exponential thickness variation

Equation 10 presents the variation of shell thickness through an exponential pattern.

$$\Delta h = \alpha e^{\left(\frac{R(\theta)-R_{min}}{R_{min}}\right)} + \beta \tag{10}$$

Accordingly, the thickness at any arbitrary point on the circumference of the ellipse with the radius of curvature of $R(\theta)$ is obtained using Equation 11.

$$h(\theta) = hmin + \alpha\left[e^{\left(\frac{R(\theta)-R_{min}}{R_{min}}\right)} - 1\right] \tag{11}$$

Considering the assumption that the cross-sectional area of the ellipse is constant, the coefficient α is obtained as B_1/B_2 where B_1 and B_2 are obtained from Equation 12.

$$\begin{aligned} B_1 &= \frac{\pi R_0 h_0}{2} - \frac{\pi R_0 hmin}{2} = \frac{\pi R_0}{2}(h_0 - hmin) \\ B_2 &= \int_0^{\frac{\pi}{2}} R(\theta)\left[e^{\left(\frac{R(\theta)-R_{min}}{R_{min}}\right)} - 1\right] d\theta \end{aligned} \tag{12}$$

2.1.3. Logarithmic thickness variation

In the case of logarithmic thickness variation, the amount of thickness increase is considered as a logarithmic distribution of the radius of curvature of the ellipse (Equation 13).

$$\Delta h = \alpha\, log\left(\frac{R(\theta)}{R_{min}}\right) + \beta \tag{13}$$

As in the previous cases, the thickness of the ellipse at any arbitrary point is obtained using Equation 14.

$$h(\theta) = hmin + \alpha\, log\left(\frac{R(\theta)}{R_{min}}\right) \tag{14}$$

Accordingly, α is obtained as C_1/C_2 where C_1 and C_2 are obtained from Equation 15.

$$\begin{aligned} C_1 &= \frac{\pi R_0 h_0}{2} - \frac{\pi R_0 hmin}{2} \\ &= \frac{\pi R_0}{2}(h_0 - hmin) \\ C_2 &= \int_0^{\frac{\pi}{2}} R(\theta)\, log\left(\frac{R(\theta)}{R_{min}}\right) d\theta \end{aligned} \tag{15}$$

2.2. Strip element formulation

In this research, five independent degrees of freedom, including three displacements (u, v and w) and two rotations (φ_θ and φ_x), were considered at each point of the shell (Figure 3). u is axial displacement in the longitudinal direction of the cylinder, v stands for displacement along the circumference of the cylinder, w represents displacement in the radial direction of the cylinder, φ_θ is rotation about the axial axis of the cylinder and φ_x represents rotation about the circumferential direction of the cylinder. Fourier series expansions and harmonic functions were employed to approximate the displacement functions in the longitudinal and transverse directions, respectively (Equation 16) [29-30].

$$\begin{aligned} u &= \sum_{p=1}^{M}\sum_{q=1}^{2} u_{pq}\,.\,cos(a_p x)\,.\,N_q(\eta) \\ &\quad + \sum_{q=1}^{2} u_{0q}\,.\,N_q(\eta).\left(\frac{1}{2} - \frac{x}{L}\right) \\ v &= \sum_{p=1}^{M}\sum_{q=1}^{2} v_{pq}.sin(\alpha_p.x).N_q(\eta) \\ w &= \sum_{p=1}^{M}\sum_{q=1}^{2} w_{pq}.sin(\alpha_p.x).N_q(\eta) \\ \varphi_x &= \sum_{p=1}^{M}\sum_{q=1}^{2} \varphi_{x_{pq}}.cos(\alpha_p.x).N_q(\eta) \\ \varphi_\theta &= \sum_{p=1}^{M}\sum_{q=1}^{2} \varphi_{\theta_{pq}}.sin(\alpha_p.x).N_q(\eta) \end{aligned} \tag{16}$$

In Equation 16, p and q stand for the harmonic number in the longitudinal direction and node number in the circumferential direction, respectively. In addition, M is the total number of harmonics and α_p is $p\pi/L$. It should be noted that the additional term considered for the u-component, relative to the other

displacements and rotations, is included in the pre-buckling analysis to accelerate convergence, but it is disregarded in the eigenvalue buckling analysis. It should be noted that, the displacement at any arbitrary point on the shell ($\overline{u}$, $\overline{v}$ and $\overline{w}$) was calculated using the first-order shear deformation theory, as expressed in Equation 17. All parameters used in Equation 17 were defined earlier [29-30].

$$\begin{aligned}\overline{u}(x.\theta.z) &= u(x.\theta) + z,\varphi_x(x.\theta)\\ \overline{v}(x.\theta.z) &= v(x.\theta) + z,\varphi_\theta(x.\theta)\\ \overline{w}(x.\theta.z) &= w(x.\theta)\end{aligned} \quad (17)$$

It should be noted that a closed, simply supported cylindrical shell is considered in this study. Accordingly, the equations corresponding to different harmonics are decoupled, thereby reducing the number of degrees of freedom in each step of the analysis. In contrast, for other boundary conditions such as fixed or free edges, the harmonics become coupled, which increases the number of degrees of freedom and consequently raises the computational cost of the model. The generalized strain and stress vectors ($\{\varepsilon\}$ and $\{\sigma\}$) are provided in Equations 18 and 19, respectively.

$$\begin{aligned}\{\varepsilon\}^T &= \{\varepsilon \quad k \quad \gamma\}\\ &= \{\varepsilon_{xx} \quad \varepsilon_{\theta\theta}\ \gamma_{x\theta}\ k_{xx} \quad k_{\theta\theta} \quad k_{x\theta} \quad \gamma_{xz} \quad \gamma_{\theta z}\}\end{aligned} \quad (18)$$

$$\begin{aligned}\{\sigma\}^T &= \{N \quad M \quad Q\}\\ &= \{N_{xx}\ N_{\theta\theta}\ N_{x\theta}\ M_{xx}\ M_{\theta\theta}\ M_{x\theta}\ Q_{xz}\ Q_{\theta z}\}\end{aligned} \quad (19)$$

In Equation 18, ε_{xx} and $\varepsilon_{\theta\theta}$ stand for the normal strains of the middle plane in the x and θ directions, respectively; $\gamma_{x\theta}$ is the shear strain in the $x\theta$ plane, k_{xx} and $k_{\theta\theta}$ are the bending curvatures about the x and θ directions, respectively; $k_{x\theta}$ represents the torsional curvature in the $x\theta$ plane, γ_{xz} and $\gamma_{\theta z}$ denote the shear strains in the xz and $x\theta$ planes in the shell thickness direction, respectively. In Equation 19, N_{xx}, $N_{\theta\theta}$ and $N_{x\theta}$ stand for the normal membrane force per unit length in the x direction, the normal membrane force per unit length in the θ direction, and the in-plane shear force in the xθ plane, respectively. In addition, M_{xx} and $M_{\theta\theta}$ represent the bending moment per unit length about the θ and x directions, respectively; $M_{x\theta}$ is the torsional moment per unit length in the xθ plane. Furthermore, Q_{xz} and $Q_{\theta z}$ stand for the out-of-plane shear forces per unit length in the xz and θz planes, respectively. The linear and nonlinear components of the strain vector were derived based on Sanders' theory and are available in the previous studies [31-32]. Sanders' theory provides sufficient accuracy for moderate thickness while accounting for transverse shear effects, which are neglected in classical thin shell theory. This makes it suitable for this study where shell thickness varies circumferentially and may reach moderate values in some regions. The generalized stress-strain relationship considered in this study is presented in Equation 20 [30].

$$\begin{Bmatrix} N \\ M \\ Q \end{Bmatrix} = \begin{bmatrix} A_{ij} & B_{ij} & 0 \\ B_{ij} & D_{ij} & 0 \\ 0 & 0 & H_{ij} \end{bmatrix} \begin{Bmatrix} \varepsilon \\ k \\ \gamma \end{Bmatrix} \quad (20)$$

In Equation 20, A_{ij} , , B_{ij} , D_{ij} and H_{ij} stand for the (i, j) components of the axial rigidity, axial-flexural coupling rigidity, flexural rigidity, and shear rigidity matrices, respectively. The mentioned rigidity matrices are determined using Equation 21 [30].

$$\begin{aligned}&\left(A_{ij}.B_{ij}.D_{ij}\right) = \int_h (1.z.z^2)\bar{Q}_{ij}(z)dz \quad i.j = 1.2.6\\ &H_{ij} = K_s \int_h \bar{Q}_{ij}(z)dz \quad i.j = 4.5\end{aligned} \quad (21)$$

In Equation 21, K_s represents the shear correction factor and was considered as $5/6$. Moreover, $\bar{Q}_{ij}(z)$ is ith and jth component of reduced stiffness matrix and is obtained using Equation 22 [30].

$$\begin{aligned}\bar{Q}_{11} &= \bar{Q}_{22} = \frac{E}{1-\nu^2}\\ \bar{Q}_{12} &= \bar{Q}_{21} = \frac{\nu E}{1-\nu^2}\\ \bar{Q}_{44} &= \bar{Q}_{55} = \bar{Q}_{66} = \frac{E}{2(1+\nu)}\end{aligned} \quad (22)$$

In Equation 22, E and v represent the modulus of elasticity and Poisson's ratio of the material, respectively. As isotropic material is utilized in this study, B_{ij} and H_{45} components are zero. The internal virtual work done by linear strains and their corresponding stresses ($\delta W_{internal}^{linear}$) was written to determine the elastic stiffness matrix of the strip element (Equation 23). Accordingly, the elastic stiffness matrix for j-th strip element and the shell ($[K_E]_j$ and $[K_E]$) were obtained from Equation 24 [29].

$$\begin{aligned}\delta W_{internal}^{linear} = \int_x \int_\theta (&N_{xx}\delta\varepsilon_{xx} + N_{\theta\theta}\delta\varepsilon_{\theta\theta} \\ &+ N_{x\theta}\delta\gamma_{x\theta} + M_{xx}\delta k_{xx} \\ &+ M_{\theta\theta}\delta k_{\theta\theta} \\ &+ M_{x\theta}\delta k_{x\theta} + Q_{xz}\delta\gamma_{xz} \\ &+ Q_{\theta z}\delta\gamma_{\theta z})R(\theta)d\theta dx\end{aligned} \quad (23)$$

$$\begin{aligned}\delta W_{internal}^{linear} &= \sum_{j=1}^{nstrip} (\delta\Delta_j)^T [K_E]_j \Delta_j \\ &= (\delta\Delta)^T K_E \Delta\end{aligned} \quad (24)$$

In Equation 24, Δ_j and Δ are displacement/rotation vectors of j-th strip element and shell, respectively. Moreover, $\delta\Delta_j$ and $\delta\Delta$ represent virtual displacement/rotation vectors of j-th element and shell, respectively. Moreover, $nstrip$ is total number of strip elements. The internal virtual work done by initial membrane forces and the nonlinear terms of membrane strains ($\delta W_{internal}^{nonlinear}$) was written to determine the geometric stiffness matrix of the strip element (Equation 25) [29, 31-32].

$$\begin{aligned}&\delta W_{internal}^{nonlinear} \\ &= \int_x \int_\theta (N_{xx}^0 \delta\varepsilon_{xx}^{nl} + N_{\theta\theta}^0 \delta\varepsilon_{\theta\theta}^{nl} \\ &+ N_{x\theta}^0 \delta\gamma_{x\theta}^{nl})R(\theta)d\theta dx\end{aligned} \quad (25)$$

The initial membrane forces (N_{xx}^0, $N_{\theta\theta}^0$, $N_{x\theta}^0$) were obtained from a pre-buckling analysis (Khayat et al., 2017). Accordingly, the geometric stiffness matrix for j-th strip element and the shell ($[K_G]_j$ and $[K_G]$) were obtained from Equation 26 [29, 31-32].

$$\begin{aligned}\delta W_{internal}^{nonlinear} &= \sum_{j=1}^{nstrip} (\delta\Delta_j)^T [K_G]_j \Delta_j \\ &= (\delta\Delta)^T K_G \Delta\end{aligned} \quad (26)$$

On other hand, the external virtual work done by the follower lateral pressure ($\delta W_{external}^{\bar{q}^l}$) was written to determine the load vector and the part of the stiffness matrix dependent on the follower lateral pressure (Equation 27) [29, 31-32].

$$\begin{aligned}\delta W_{external}^{\bar{q}^l} &= \delta W_{external}^{\bar{q}} + \\ &\delta W_{sym.}^{domain} + \delta W_{skew}^{load} + \delta W_{skew}^{bound}\end{aligned} \quad (27)$$

In Equation 27, $\bar{q}^l$ is follower lateral pressure and $\bar{q}$ represents non-follower part of the lateral pressure. As presented in Equation 27, $\delta W_{external}^{\bar{q}^l}$ involves four parts including $\delta W_{external}^{\bar{q}}$, $\delta W_{sym.}^{domain}$, δW_{skew}^{load} and δW_{skew}^{bound} which are obtained from Equations 28 to 31, respectively [29, 31-32]. The force vector of the model is obtained using the external work done by non-follower part of the lateral pressure ($\delta W_{external}^{\bar{q}}$). On other hand, $\delta W_{sym.}^{domain}$, δW_{skew}^{load} and δW_{skew}^{bound} depend on follower part of the lateral pressure [29, 31-32].

$$\delta W_{external}^{\bar{q}} = -\int_0^{2\pi}\int_0^{L} \bar{q}(x.\theta)\,\delta w\, R(\theta) dx\, d\theta \quad (28)$$

$$\delta W_{sym,}^{domain} = -\delta \iint_A \frac{1}{2}\bar{q}^l(x.\theta)(v^2 + w^2 + w\,R(\theta)\frac{\partial u}{\partial x} - R(\theta)\,u\frac{\partial w}{\partial x} + w\frac{\partial v}{\partial \theta} - v\frac{\partial w}{\partial \theta})\, dx\, d\theta \quad (29)$$

$$\delta W_{skew}^{load} = -\iint_A (-w\delta v\frac{\partial \bar{q}^l}{\partial \theta} + v\,\delta w\frac{\partial \bar{q}^l}{\partial \theta} - R(\theta)w\,\delta u\frac{\partial \bar{q}^l}{\partial x} + R(\theta)\,u\,\delta w\,\frac{\partial \bar{q}^l}{\partial x})\, dx\, d\theta \quad (30)$$

$$\delta W_{skew}^{bound} = \frac{1}{2}\int_0^{2\pi}(R(\theta)w\,\delta u\,\bar{q}^l - R(\theta)u\,\delta w\,\bar{q}^l)\Big|_0^L d\theta + \frac{1}{2}\int_0^{L}(w\,\delta v\,\bar{q}^l - v\,\delta w\bar{q}^l)\Big|_0^{2\pi} dx \quad (31)$$

Generally, the pressure exerted by the water on a structure wall varies in the circumferential and longitudinal directions. So, in Equations 27 and 29, δW_{skew}^{load} depends on variation of follower lateral pressure in θ and x directions. As in this study, $\bar{q}^l$ was constant along with θ and x directions, δW_{skew}^{load} is zero. Moreover, δW_{skew}^{bound} in Equations 27 and 31 depend on boundary conditions of the shell and as a closed simply supported cylindrical shell was considered in this study, δW_{skew}^{bound} is zero [29, 31-32]. In this study, $\delta W_{sym.}^{domain}$ is the only non-zero term of external virtual work done by follower lateral pressure and has a quadratic form. Accordingly, the load stiffness matrices of j-strip element and shell ($[K_P]_j$ and $[K_P]$) were obtained using $\delta W_{sym.}^{domain}$ (Equation 32) [29, 31-32].

$$\delta W_{sym.}^{domain} = \sum_{j=1}^{nstrip}(\delta\Delta_j)^T[K_P]_j\Delta_j = (\delta\Delta)^T K_P\Delta \quad (32)$$

Equation 33 were utilized to calculated the mode shapes (ϕ) of the shell based on the eigenvalue problem [29, 31-32].

$$(K_E - \lambda(K_G + K_P))\phi = 0 \quad (33)$$

In Equation 33, K_E, K_G and K_p are elastic, geometrical and follower pressure-dependent of stiffness matrices of the shell, respectively. It should be noted that K_p stiffness matrix in the follower and non-follower pressure states is non-zero and zero, respectively. It should be noted that the Gauss numerical integration method (Gaussian quadrature) was adopted in this research.

3. Model convergence and validation

In this section, the convergence as well as the accuracy of the results obtained from the model developed in this research are examined.

3.1. Model convergence

An isotropic elliptical cylindrical shell with b/a ratios of 0.5, 0.7, and 0.9 was considered to evaluate the convergence of the model developed in this study. The shell has a variable thickness following an exponential pattern and is subjected to a follower lateral pressure. The Young's modulus of the shell material is 2000 kN/mm², and the Poisson's ratio is 0.3. Moreover, hmin was considered as 0.48. Figure 5 illustrates the convergence of the model results as the total number of nodes increases from 48 to 120. The relative error was calculated based on the buckling load obtained for the 120-node case. As shown in Figure 5, increasing the number of nodes reduces the difference between results to below 0.1%. Moreover, the figure indicates that as the b/a ratio decreases, the model requires a larger number of nodes to achieve

good convergence. Consequently, for all b/a values, the model with 120 nodes provides sufficiently converged results.

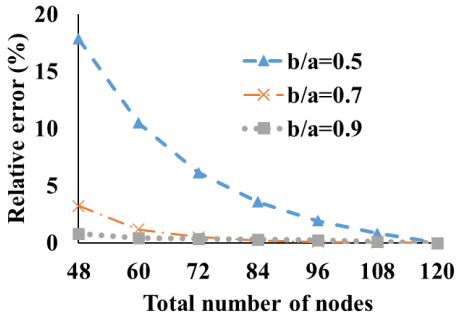
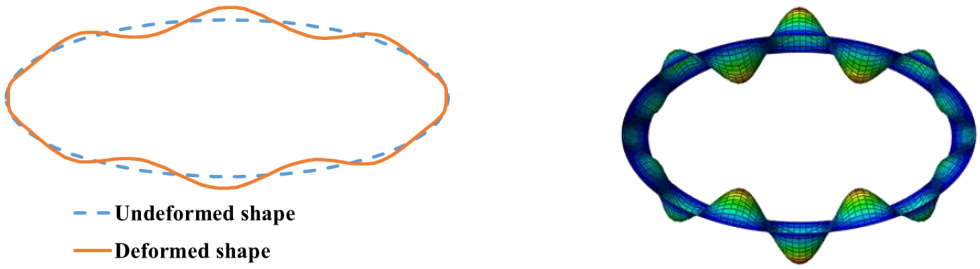


Figure 5. Convergence of model developed in this study

3.2. Model validation

A comparison was made between results obtained from the model developed in this study and those of finite element model implemented in ABAQUS to validate the developed model. In this regard, an elliptical cylindrical shell with a power-law thickness variation (power = 0.5), subjected to follower lateral pressure and made of isotropic material (as described in the previous sub-section), was analyzed using both the developed model and the well-known finite element software ABAQUS. The ratio of cylinder length to equivalent radius (L/R_0), minimum thickness (hmin), and b/a were set to 1, 0.48, and 0.5, respectively. The buckling loads obtained from the developed model and ABAQUS were 0.012587 and 0.012027, respectively, indicating a small difference of 4.6%. Furthermore, as shown in Figure 6, the buckling mode shapes obtained from the developed model closely match those predicted by ABAQUS. This indicates the acceptable accuracy of the results obtained from the numerical model developed in this study.



(a) (b)

Figure 6. Mode shapes of shell obtained from (a) model developed in this study (b) ABAQUS

4. Parametric study

A parametric study was conducted to investigate the effects of various parameters on the buckling load of the shell, including the TVP, minimum thickness (hmin), shell geometric characteristics, properties of the functionally graded material, and loading type (follower and non-follower lateral pressures). Based on this study, the ratio of shell length to equivalent radius (L/R_0) was considered as 0.5, 1, 2, 4, 8, 16, and 32. The shell thickness was varied between 0.35 and 1, and the ratio of the minimum to maximum diameters of the oval section (b/a) ranged from 0.4 to 1. It

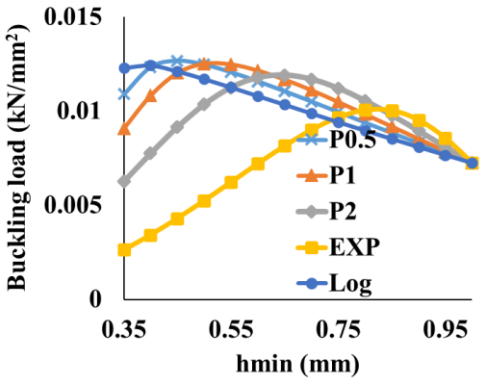
should be noted that logarithmic, exponential, and power variation-thickness patterns are represented by the parameters "Log", "EXP", and "P", respectively. Also, for the power thickness-variation pattern, the power value appears in front of the "P". In the analyses, the shell structure was discretized into 120 curved two-node strip elements, all of which were identical. The results of the parametric study are presented in the following sub-sections.

4.1. Minimum thickness

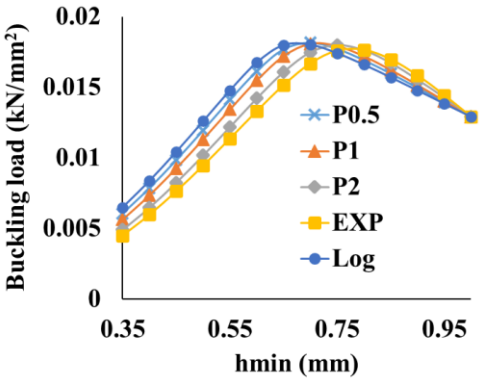
The effect of minimum thickness (hmin) on the buckling load of the shell under follower lateral pressure, considering different TVPs, was investigated. In this section, hmin was varied between 0.35 and 1 mm and L/R_0 is assumed to be equal to 1. Figure 7 shows the effect of variation of minimum thickness (hmin) on the buckling load of a variable- thickness shell with different values of b/a under follower and non-follower lateral pressures. The value of b/a in figures 7(a) to 7(c) is 0.5, 0.7, and 0.9, respectively.

As shown in Figure 7, in all cases, increasing hmin from 0.35 to a certain value (hereinafter referred to as the optimum value) leads to a maximum buckling load. When hmin exceeds this optimum value, the buckling load of the shell decreases in all cases. According to figure 7, the optimum value of hmin depends on two factors: b/a ratio and the TVP. Based on the results shown in Figures 7, as the b/a ratio increases (from 0.5 to 0.9), the influence of TVP on both the optimum value of hmin and the buckling load of the shell decreases significantly. For example, in the case of an ellipse with a b/a ratio of 0.9 (Figure 7(c)), there is only a slight difference between the results obtained for all TVPs, whereas for a b/a ratio of 0.5 (Figure 7(a)), this difference is quite substantial. Figure 7 indicates that the power-law TVP with a power of 0.5 yields the highest buckling load across all b/a ratios. This is followed by the power-law TVP with a power of 1 and the logarithmic TVP, which also produce relatively high buckling loads. It should be noted that the optimum hmin varies depending on the selected TVP and b/a ratio.

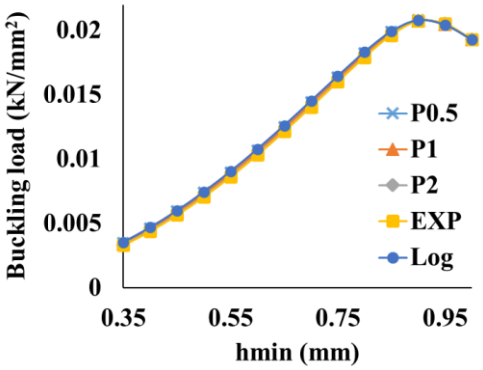
To gain a deeper understanding of how minimum thickness variation influences the buckling behavior of a variable-thickness shell under follower lateral pressure, the first mode shape of an elliptical shell with a b/a ratio of 0.5, a power-law TVP (with a power of 1), and different minimum thickness values is shown in Figure 8. As illustrated in this figure, when hmin reaches its optimum value (i.e., 0.51), general buckling occurs, meaning the entire shell wall deforms during buckling. In contrast, for other minimum thickness values, only regions of the shell wall with lower bending stiffness (i.e., those with a larger radius of curvature) undergo local deformation during buckling.



(a)



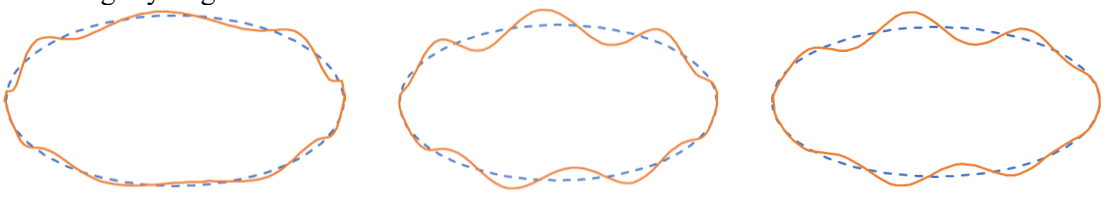
(b)



(c)

Figure 7. Effect of variation of minimum thickness on buckling load of thickness-variable shell with different values of b/a under follower lateral pressure (a) b/a=0.5 (b) b/a=0.7, (c) b/a=0.9

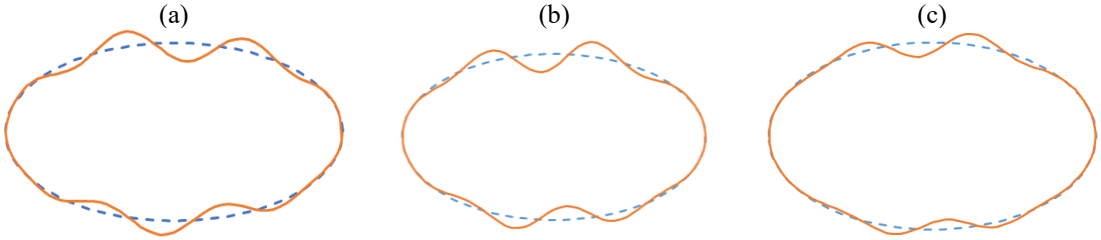
This indicates that when hmin reaches its optimum value, the continuous thickness variation around the elliptical shell circumference results in a more uniform distribution of bending stiffness. As a result, the entire elliptical shell wall buckles simultaneously (occurrence of general buckling). However, in an elliptical shell with constant thickness, the bending stiffness is lower in regions with a larger radius of curvature, leading to localized buckling in those areas. Although the buckling loads obtained from the Power (P), EXP, and Log TVPs are close, the power one consistently yields slightly higher critical loads. This improvement can be attributed to the smoother circumferential thickness distribution in the power pattern, which provides better alignment between thickness variation and curvature changes. As a result, the shell's bending stiffness is enhanced and localized stress concentrations are reduced in the power case. These observations indicate that an optimum power exponent may exist that maximizes the buckling load for a given shell configuration. Exploring this optimum value and its influence on shell stability represents a promising direction for future research.



Buckling load = 0.0113 kN/mm²
(a)

Buckling load = 0. 0126 kN/mm²
(b)

Buckling load = 0. 0118 kN/mm²
(c)



Buckling load = 0. 0108 kN/mm²
(d)

Buckling load = 0. 0093 kN/mm²
(e)

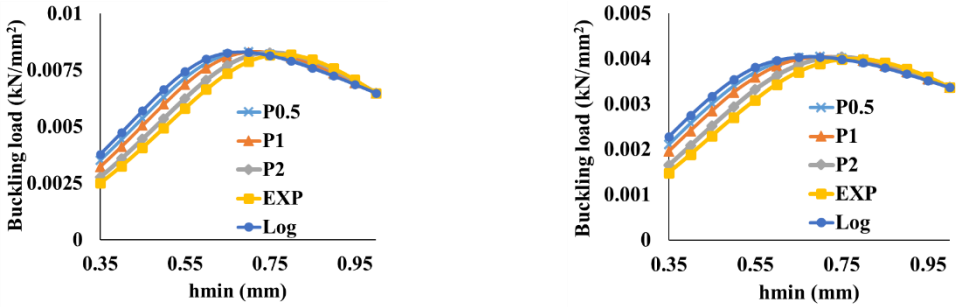
Buckling load = 0. 0081 kN/mm²
(f)

Figure 8. Effect of hmin on first mode shape of elliptical shell with b/a of 0.5 and power-law TVP (a) hmin = 0.4, (b) hmin = 0.51, (c) hmin = 0.6, (d) hmin = 0.7, (e) hmin = 0.8, (f) hmin = 0.9

It should be noted that eigenvalue buckling analyses were performed for different harmonic numbers to calculate the longitudinal half-wave associated with buckling under lateral pressure. The harmonic number corresponding to the minimum buckling pressure was designated as the longitudinal buckling mode. In this study, all longitudinal buckling modes for different geometries and material properties consisted of a single half-wave.

4.2. Ratio of shell length to equivalent radius (L/R_0)

Figure 9 shows the effect of the length to equivalent radius ratio (L/R_0) of 2 and 4, respectively, on the influence of minimum thickness on the buckling load of isotropic thickness-variable shell with b/a of 0.7 under follower lateral pressure. The trend of the results shown in Figure 9 is the same as the results presented in the previous sub-section. Moreover, according to Figure 9, although increasing L/R_0 does not significantly change the optimum value of hmin, it causes a significant reduction in the buckling load of the shell.



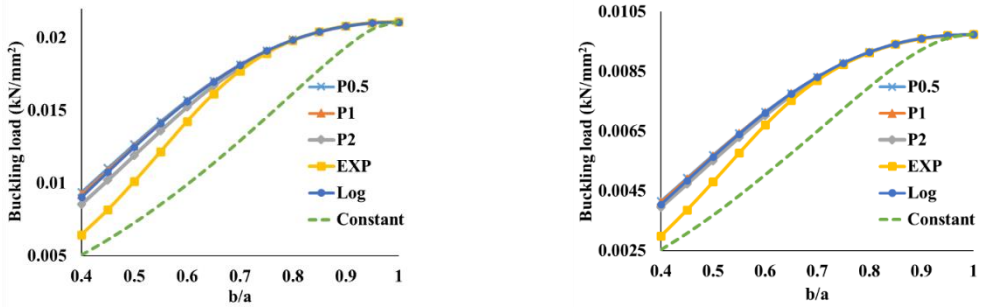
(a) (b)

Figure 9. Effect of variation of minimum thickness on buckling load of thickness-variable shell with b/a of 0.7 and different values of L/R_0 under follower lateral pressure (a) $L/R_0 = 2$ (b) $L/R_0 = 4$

As shown in Figure 9, for all cases, when hmin reaches its optimum value, the buckling load of the shell reaches its maximum value. In cases having optimum hmin, the shell undergoes general buckling, whereas in other cases, local deformations occur in limited regions of the shell.

4.3. Minimum to maximum diameters ratio of oval section (b/a)

The effect of the minimum-to-maximum diameter ratio of the oval section (b/a) on the buckling load of thickness-variable shells with optimum hmin and different values of L/R_0 ratio (2 and 4) under follower lateral pressure is shown in Figure 10.



(a) (b)

Figure 10. Effect of variation of b/a on buckling load of thickness-variable shell with optimum hmin and different L/R_0 values under follower lateral pressure (a) $L/R_0 = 2$ (b) $L/R_0 = 4$

The results indicate that applying a TVP in the elliptical shells can significantly increase the buckling load compared to shells with constant thickness, especially at lower b/a ratios. As the b/a ratio increases, the differences in buckling loads among various TVPs decrease, and the buckling load converge toward similar values. It indicates that applying a proper TVP on the circumferential direction is a suitable approach for enhancing the buckling load of elliptical cylindrical shells.

An index presenting the percentage Improvement in the Buckling Load (IBL) obtained for the shells having TVP compared to the constant thickness cases was defined to gain a deeper understanding of the effect of TVP on enhancement of buckling load of the elliptical shell under lateral follower pressure (Equation 34).

$$IBL = \frac{P_{Variable\ thickness} - P_{constant\ thickness}}{P_{constant\ thickness}} \times 100 \quad (34)$$

In Equation 34, $P_{Variable-thickness}$ and $P_{\text{constant thickness}}$ stand for the buckling loads of the thickness-variable and thickness-constant shells under lateral follower pressure. Figure 11 shows the effect of TVP on enhancement of buckling load of elliptical shell with different b/a values. In this figure, the ratio of L/R_0 is considered as 2 and 4. According to Figure 11, as L/R_0 ratio increases from 2 to 4, the effect of TVP on enhancement of buckling load decreases for all cases of b/a and TVP. For instance, the maximum IBL for L/R_0 ratios of 2 and 4 is about 36 and 65 percent, respectively. As depicted in Figure 11, the power-law TVP with power of 0.5 stands for the best TVP for enhancing the buckling load of elliptical shell.

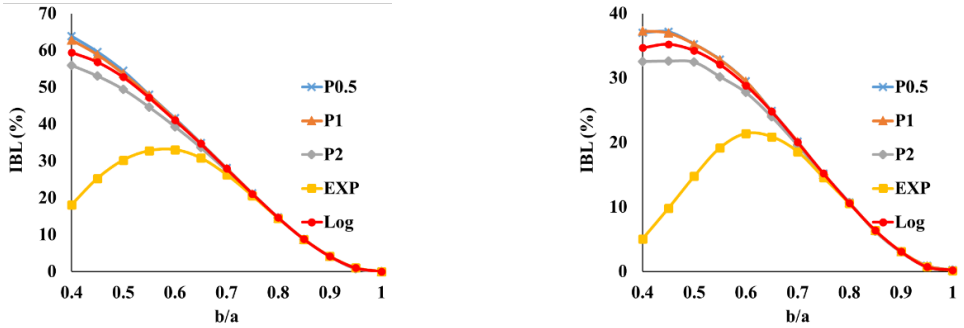


Figure 11. Effect of TVP on enhancement of buckling of elliptical shell with different b/a values under follower lateral pressure (a) $L/R_0 = 2$ (b) $L/R_0 = 4$

4.5. Lateral pressure type (follower or non-follower)

In this section, the effect of lateral pressure type (follower or non-follower) on the buckling behavior of a thickness-variable shell with the optimal hmin is evaluated. To reach a deep understanding of the influence of TVP on the difference between buckling loads of the shell under follower and non-follower pressures, firstly, the effect of b/a ratio on the difference between the buckling loads of a constant-thickness shell under follower and non-follower loads (considering L/R_0 of 8) is shown in Figure 12. The results presented in Figure 12 show that in the case of a shell with constant thickness, there is a significant difference between the buckling loads obtained for the shell under follower and non-follower pressures. This difference increases significantly with increasing b/a ratio. In order to investigate the effect of TVPs on this difference, the index defined in Equation 35 is calculated.

$$BLRD\% = \left|\frac{P_{follower\ pressure} - P_{non-follower\ pressure}}{P_{follower\ pressure}}\right| \times 100 \quad (35)$$

In Equation 35, BLRD stands for Buckling Load Relative Difference, $P_{follower\ pressure}$ is buckling load of the shell under follower pressure and $P_{non-follower\ pressure}$ represents the buckling load of the shell under non-follower pressure. The BLRD indicates the percentage difference between the buckling loads of the shell under the follower and non-follower pressures.

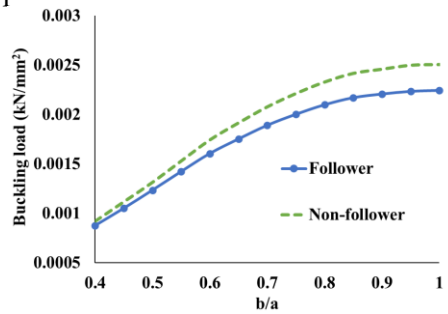


Figure 12. Effect of b/a ratio on the difference between the buckling loads of a constant-thickness shell under follower and non-follower loads (L/R_0 of 8)

Table 1 the effects of L/R_0, b/a and TVP on BLRE. As presented in this table, the BLRD increases for constant-thickness case and all TVPs and b/a ratios, as L/R_0 ratio increases. The rate of change in BLRD depends on the value of L/R_0; it is significantly higher when L/R_0 is between 8 and 16, compared to when it is less than 8 or greater than 16. Consequently, the maximum BLRD, approximately 35 percent, is observed at the highest values of both L/R_0 and b/a. According to Table 1, the lowest value of BLRD corresponds to the constant thickness pattern in all cases, while the highest BLRD, approximately 30%, is associated with the logarithmic TVP. Notably, the differences in BLRD among the various TVPs decrease significantly, as the b/a ratio increases. The BLRD values obtained for different TVPs show no significant differences at a b/a ratio of 0.9. This issue highlights the noticeable effect of TVPs on the buckling behavior of elliptical shells with smaller b/a ratios.

Table 1. Effects of L/R_0, b/a ratio and thickness variation pattern on BLRD

TVP	L/R \ b/a	0.4	0.5	0.6	0.7	0.8	0.9	1.0
Constant	1	0.11	0.19	0.27	0.41	0.55	0.73	0.91
	4	1.01	1.47	2.15	3.02	3.98	5.12	5.75
	8	2.51	3.68	5.42	7.30	9.35	10.99	11.65
	16	6.87	11.03	15.23	20.25	27.35	30.65	31.69
Power 0.5	1	0.53	0.67	0.75	0.85	0.87	0.90	0.91
	4	2.38	3.56	4.14	5.20	5.48	5.71	5.75
	8	3.87	6.36	8.20	9.98	10.83	11.95	11.65
	16	12.63	15.15	21.21	23.59	30.35	30.96	31.69
EXP	1	0.17	0.26	0.52	0.77	0.85	0.89	0.91
	4	1.17	2.21	3.64	4.72	5.42	5.62	5.75
	8	2.49	4.43	7.05	9.63	10.82	11.49	11.65
	16	7.19	10.97	15.80	22.24	29.04	31.45	31.69
Log	1	0.49	0.62	0.75	0.85	0.88	0.90	0.91
	4	2.42	3.63	4.46	5.13	5.50	5.64	5.75
	8	4.78	6.31	8.52	9.88	11	10.78	11.65
	16	14.84	16.81	20.64	28.13	28.57	31.17	31.69

5. Conclusions

A review of the previous studies shows that, the buckling load of elliptical cylindrical shells subjected to follower lateral pressure is significantly lower than that of the circular shell due to the uniform curvature of circular cross-sections. In this study, to enhance the buckling capacity of elliptical shells, the shell thickness is varied smoothly along the circumferential direction, with greater thickness assigned to regions of lower curvature. Three Thickness Variation Patterns (TVPs) (including power-law, exponential, and logarithmic) were considered in this study. A finite strip model of the shell was developed, and the buckling load was determined using the eigenvalue method. The accuracy of the developed model was validated by comparison with results obtained from finite element analysis. A comprehensive parametric study was conducted to assess the effect of geometric parameters and TVPs on the buckling of elliptical shells with circumferentially variable thickness. The main results obtained from the parametric study are summarized below:

- Despite keeping the material volume constant, the buckling load of thickness-variable elliptical shell is significantly higher than that of the constant thickness ones (up to 2 times).
- By increasing minimum to maximum diameters ratio of oval section (b/a) and length to equivalent radius ratio (L/R_0), the effect of TVP on enhancement of buckling load of the thickness-variable elliptical shell decreases.
- In all TVPs, the maximum buckling load was achieved when the minimum thickness of the elliptical shell (hmin) reaches an optimal value.
- As b/a ratio decreases, the optimal value of hmin decreases for all TVPs.

Funding Statement

This research was funded by Shahid Chamran University of Ahvaz, grant number SCU.C1403.530. The authors are grateful for the financial support provided.

Conflict of Interest

The authors declare that they have no conflict of interest.

AI Statement

The author(s) did not use AI tools for conducting this research.

Author Contributions

All authors contributed to the study conception, design, material preparation, analysis, writing first draft and final version of the manuscript.

References

1. Khajehdezfuly A, Poorveis D, Nazarinia S. Comparison between linear and nonlinear buckling loads of FGM cylindrical panel with cutout. Int J Non Linear Mech. 2023;150:104361.
2. Poorveis D, Khajehdezfuly A, Moradi S, Shirshekan E. A simple spline finite strip for buckling analysis of composite cylindrical panel with cutout. Lat Am J Solids Struct. 2019;16:e227.
3. Poorveis D, Khajehdezfuly A, Moradi S. Effects of position and shape of cutout on the axial buckling load of composite cylindrical panel. Amirkabir J Mech Eng. 2019;52(10):2879-98.
4. Tabish FNU, Mamaghani IHP. Buckling behavior and design optimization of stiffened-aluminum cylindrical shells under external pressure. J Struct Des Constr Pract. 2025;30(2):04025006.
5. Khan S, Kumar A. Buckling behaviour for advance cylindrical shells (COPV) subjected to extreme pressure conditions: A comprehensive review. Polym Compos. 2025.
6. Fazlalipour N, Ghanbari-Ghazijahani T, Showkati H. A review of buckling capacity of steel cylindrical shells under external pressure: reinforcements and imperfections (2005–Present). Thin-Walled Struct. 2025;113475.
7. Aksogan O, Sofiyev AH. Dynamic buckling of a cylindrical shell with variable thickness subject to a time-dependent external pressure varying as a power function of time. J Sound Vib. 2002;254(4):693-702.
8. Jabbari M, Nejad MZ, Ghannad M. Thermo-elastic analysis of axially functionally graded

rotating thick cylindrical pressure vessels with variable thickness under mechanical loading. Int J Eng Sci. 2015;96:1-18.
9. Fan H, Chen Z, Cheng J, Huang S, Feng W, Liu L. Analytical research on dynamic buckling of thin cylindrical shells with thickness variation under axial pressure. Thin-Walled Struct. 2016;101:213-21.
10. Ghareghani S, Loghman A, Mohammadimehr M. Analysis of FGM micro cylindrical shell with variable thickness using Cooper Naghdi model: bending and buckling solutions. Mech Res Commun. 2021;115:103739.
11. Bacciocchi M, Eisenberger M, Fantuzzi N, Tornabene F, Viola E. Vibration analysis of variable thickness plates and shells by the generalized differential quadrature method. Compos Struct. 2016;156:218-37.
12. Aghajari S, Abedi K, Showkati H. Buckling and post-buckling behavior of thin-walled cylindrical steel shells with varying thickness subjected to uniform external pressure. Thin-Walled Struct. 2006;44(8):904-9.
13. Chen Z, Yang L, Cao G, Guo W. Buckling of the axially compressed cylindrical shells with arbitrary axisymmetric thickness variation. Thin-Walled Struct. 2012;60:38-45.
14. Selahi E, Setoodeh AR, Tahani M. Three-dimensional transient analysis of functionally graded truncated conical shells with variable thickness subjected to an asymmetric dynamic pressure. Int J Press Vessel Pip. 2014;119:29-38.
15. Sofiyev AH. The buckling of an orthotropic composite truncated conical shell with continuously varying thickness subject to a time dependent external pressure. Compos Part B Eng. 2003;34(3):227-33.
16. Ghannad M, Rahimi GH, Nejad MZ. Elastic analysis of pressurized thick cylindrical shells with variable thickness made of functionally graded materials. Compos Part B Eng. 2013;45(1):388-96.
17. Fazlalipour N, Showkati H. Geometric properties and imperfections influence on buckling behavior of variable-thickness steel cylindrical shells subjected to combined loading: experimental and numerical study. Structures. 2023;55:834-52.
18. Bakulin VN, Nedbai AY. Dynamic stability of a composite cylindrical shell with linear-variable thickness under pulsed external pressure. J Eng Phys Thermophys. 2021;94(2):525-33.
19. Mahboubi Nasrekani F, Eipakchi H. Axisymmetric buckling of cylindrical shells with nonuniform thickness and initial imperfection. Int J Steel Struct. 2019;19:435-45.
20. Ghasemi AR, Hajmohammad MH. Evaluation of buckling and post buckling of variable thickness shell subjected to external hydrostatic pressure. J Solid Mech. 2017;9(2):239-48.
21. Khalifa Ahmed M. Elastic buckling behaviour of a four-lobed cross section cylindrical shell with variable thickness under non-uniform axial loads. Math Probl Eng. 2009;2009(1):829703.
22. Khalifa Ahmed M. A new vibration approach of an elastic oval cylindrical shell with varying circumferential thickness. J Vib Control. 2012;18(1):117-31.
23. Gusic G, Combescure A, Jullien JF. The influence of circumferential thickness variations on the buckling of cylindrical shells under external pressure. Comput Struct. 2000;74(4):461-77.
24. Yang L, Luo Y, Qiu T, Yang M, Zhou G, Xie G. An analytical method for the buckling analysis of cylindrical shells with non-axisymmetric thickness variations under external pressure. Thin-Walled Struct. 2014;85:431-40.
25. Feng WZ, Chen ZP, Jiao P, Zhou F, Fan HG. Buckling of cylindrical shells with arbitrary circumferential thickness variations under external pressure. J Mech. 2017;33(1):55-64.
26. Yang L. Analytical study on the buckling of cylindrical shells with circumferential thickness variation under varying external pressure. J Press Vessel Technol. 2024;146(4).
27. Birman V, Simitses GJ. Elliptical and circular cylindrical sandwich shells with different facings. J Sandwich Struct Mater. 2000;2(2):152-76.
28. Silvestre N. Buckling behaviour of elliptical cylindrical shells and tubes under compression. Int J Solids Struct. 2008;45(16):4427-47.
29. Moradi A, Poorveis D, Khajehdezfuly A. Buckling of FGM elliptical cylindrical shell under follower lateral pressure. Steel Compos Struct. 2022;175-91.
30. Poorveis D, Khajehdezfuly A, Sardari MR, Moradi S. An accurate approach for buckling analysis of stringer stiffened laminated composite cylindrical shells under axial

compression. Steel Compos Struct. 2024;51(5):545.
31. Khayat M, Poorveis D, Moradi S, Hemmati M. Buckling of thick deep laminated composite shell of revolution under follower forces. Struct Eng Mech. 2016;58(1):59-91.
32. Khayat M, Poorveis D, Moradi S. Buckling analysis of functionally graded truncated conical shells under external displacement-dependent pressure. Steel Compos Struct. 2017;23(1):1-16.



© 2025 by the authors. Licensee SCU, Ahvaz, Iran. This article is an open access article distributed under the terms and conditions of the Creative Commons Attribution 4.0 International (CC BY 4.0 license) (http://creativecommons.org/licenses/by/4.0/).